Cell Reports, Volume *23*

Supplemental Information

Removing 4E-BP Enables Synapses to Refine without Postsynaptic Activity

Yumaine Chong, Natasha Saviuk, Brigitte Pie, Nathan Basisty, Ryan K. Quinn, Birgit Schilling, Nahum Sonenberg, Ellis Cooper, and A. Pejmun Haghighi

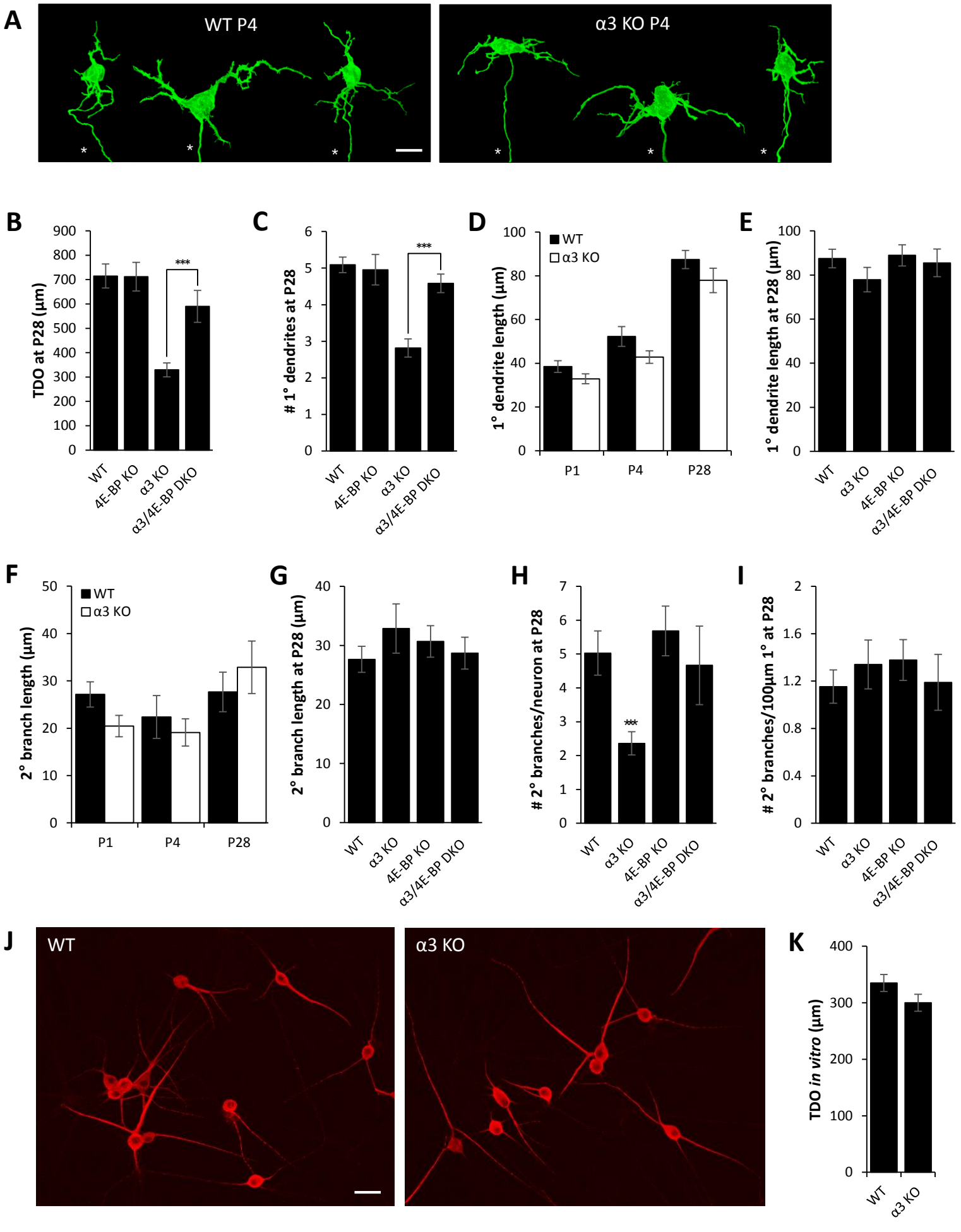

Fig. S1 Chong *et al.*

Figure S1. Dendritic morphology of WT, α3 KO, 4E-BP KO, and α3/4E-BP DKO SCG neurons. Related to Figure 3.

Lipophilic dye, DiO, was applied to the postganglionic nerve of the SCG to sparsely label a random subset of individual SCG neurons. Neurons were imaged with confocal microscopy and reconstructed in 3D to quantify the length and number of dendritic branches.

(**A**) Maximum intensity projections of DiO-labelled P4 neurons from WT (left) and α3 KO (right) SCG. All neurons are shown at the same scale. Scale bar, 20 μm; axons are marked by an asterisk.

(**B**&**C**) P28 SCG neuron; (**B**) Average total dendritic outgrowth, (**C**) average number of primary dendrites.

(**D**) Average length of primary dendrites at P1, P4, and P28; WT (filled columns), α3 KO (open columns).

(**E**) Average length of primary dendrites per P28 SCG neuron.

(**F**) Average length of secondary dendrites at P1, P4, and P28; WT (filled columns), α3 KO (open columns).

(**G**-**I**) P28 SCG neuron; (**G**) Average length of secondary branches, (**H**) average number of secondary branches, (**I**) average number of secondary branches normalized to 100μm length of primary dendrite.

Error bars represent ± SEM; ***p<0.001. WT: for P1, n=23 neurons (10 mice); for P4, n=28 neurons (10 mice); and for P28, n=34 neurons (12 mice). α3 KO: for P1, n=21 neurons (10 mice); for P4, n=24 neurons (10 mice); and for P28, n=36 neurons (14 mice). For 4E-BP KO at P28, n=22 neurons (8 mice). For α3/4E-BP DKO at P28, n=24 neurons (6 mice).

(**J**) Immunostaining for MAP-2 labels dendrites of cultured P4 neurons (14 days *in vitro*) from WT SCG (left) and α3 KO SCG (right). Scale bar, 40 μm.

(**K**) Average total dendritic outgrowth per cultured SCG neuron after 14 days *in vitro*.

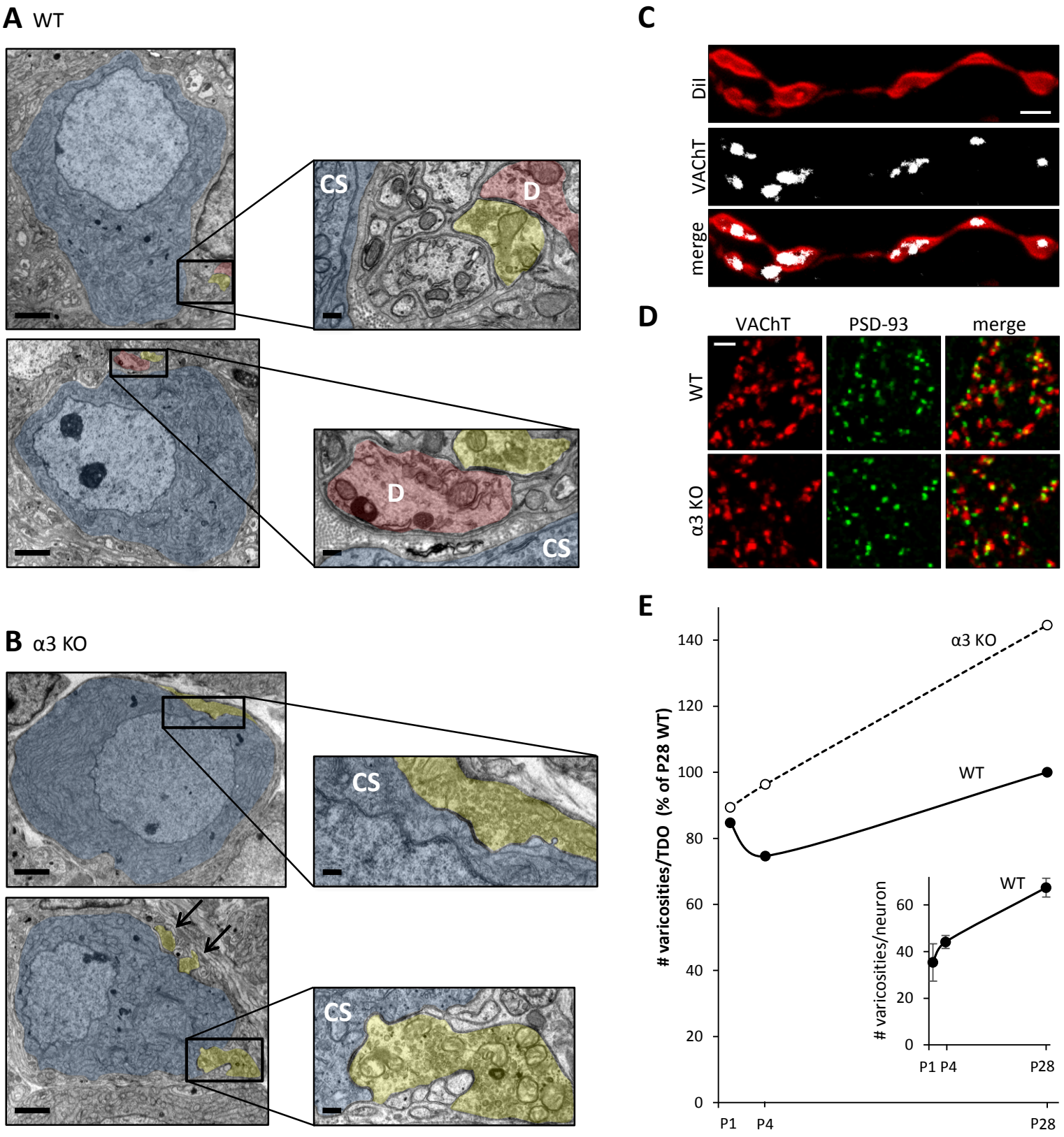

Fig. S2 Chong *et al.*

Figure S2. Varicosities in α3 KO SCG are larger and border the cell soma more frequently than in WT SCG. Varicosities have VAChT, which colocalizes with PSD-93. Related to Figure 3.

(**A**&**B**) Sample electron micrographs show cell somas (blue), varicosities (yellow) and dendrites (red). Low power images (left) show the cell soma in its entirety; scale bar, 2 μm. Boxed regions are magnified on the right; scale bar, 0.2 μm. In WT sections (A), varicosities were predominantly found in the neuropil between cell somas. In α3 KO sections (B), varicosities bordering the cell soma were often larger than those in WT sections. Arrows in the lower α3 KO micrograph point to two additional varicosities on the cell soma.

(**C**) Confocal image of a DiI-labeled axon (red), immunostained for VAchT. Varicosities are positive for VAChT (white). Scale bar, 2 μm.

(**D**) Confocal images SCG sections immunostained for VAChT (red) and PSD-93 (green). Over 90% of presynaptic VAChT puncta are colocalized with postsynaptic PSD-93 puncta; scale bar, 3 μm. Images were selected from the neuropil area between cell bodies where synapse concentration is highest.

(**E**) Number of varicosities normalized to total dendritic outgrowth for WT neurons and α3 KO neurons at P1, P4 and P28. Inset shows the number of varicosities for WT SCG neurons, which increases over 2-fold from P1 to P28. For P1, n=6 neurons (3 mice); for P4, n=9 neurons (5 mice); and for P28, n=10 neurons (4 mice).

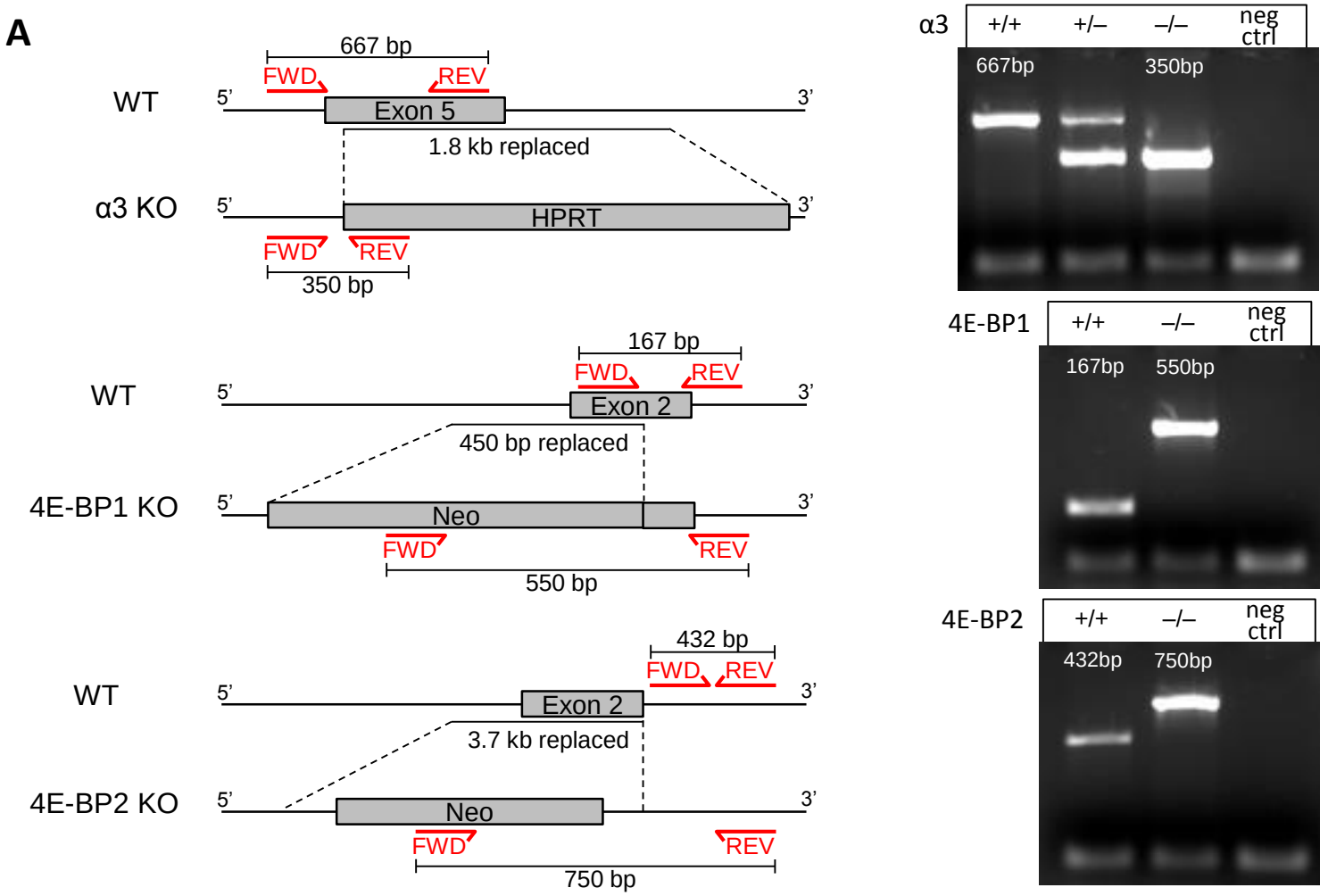

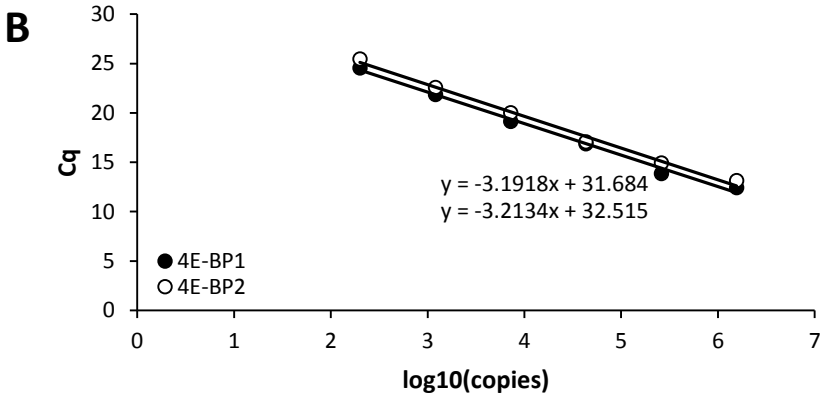

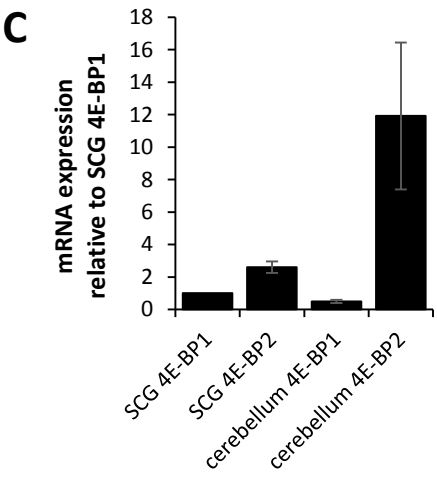

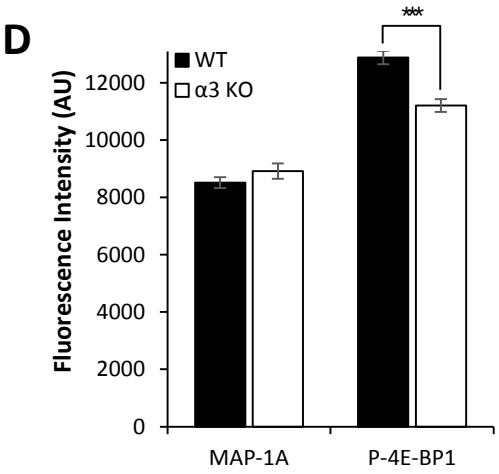

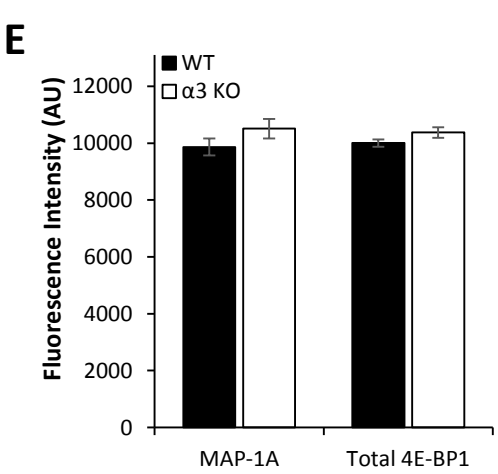

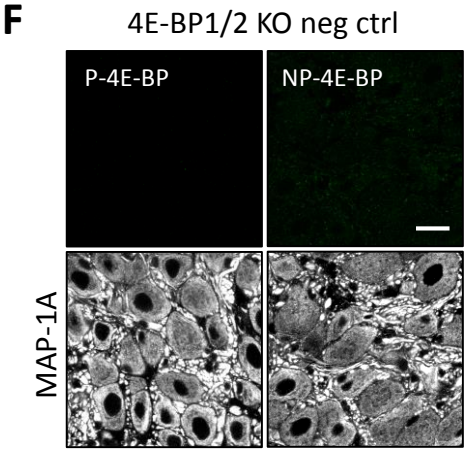

Fig. S3 Chong *et al.*

Figure S3. 4E-BP1 and 4E-BP2 are both expressed in SCG, and WT SCG has higher levels of P-4E-BP1 than α3 KO SCG. Related to Figure 4.

(**A**) Genotypes of α3, 4E-BP1 and 4E-BP2 KO mice were determined by PCR. Left: Diagrams show WT and KO alleles for α3, 4E-BP1 and 4E-BP2. The binding locations of the primers used for genotyping for indicated in red. See Table S1 for primer sequences. Right: Figures show PCR amplicons run on an agarose gel; numbers above each band correspond to expected amplicon sizes.

(**B**&**C**) Standard curves were generated from a 6-point serial dilution of known copy numbers of 4E-BP1 and 4E-BP2 cDNA (B). Primer pairs for each transcript have a near-identical amplification efficiency. Overlapping standard curves indicate that both primer pairs function in a comparable manner. Average 4E-BP1 and 4E-BP2 mRNA levels expressed in SCG and cerebellum (C). The ratios of 4E-BP1:4E-BP2 mRNA levels are ~1/2.6 in SCG and ~1/24 in cerebellum. For SCG, n=8 mice and for cerebellum n=8 mice. See Table S2 for primer sequences.

(**D**&**E**) Mean fluorescence intensity of MAP-1A, P-4E-BP1 and total 4E-BP1 in WT and α3 KO SCG; (**D**) MAP-1A and P-4E-BP1 and (**E**) MAP-1A and total 4E-BP1.

Error bars represent ± SEM; ***p<0.001. For B, WT n=120 neurons (3 mice), α3 KO n=120 neurons (3 mice). For C, WT n=140 neurons (3 mice), α3 KO n=140 neurons (3 mice).

(**F**) 4E-BP1/2 KO SCG at P28 were immunostained for phospho-4EBP1 and total 4E-BP1 (green) and MAP-1A (white) to test for non-specific binding of antibodies. Scale bar, 20 μm.

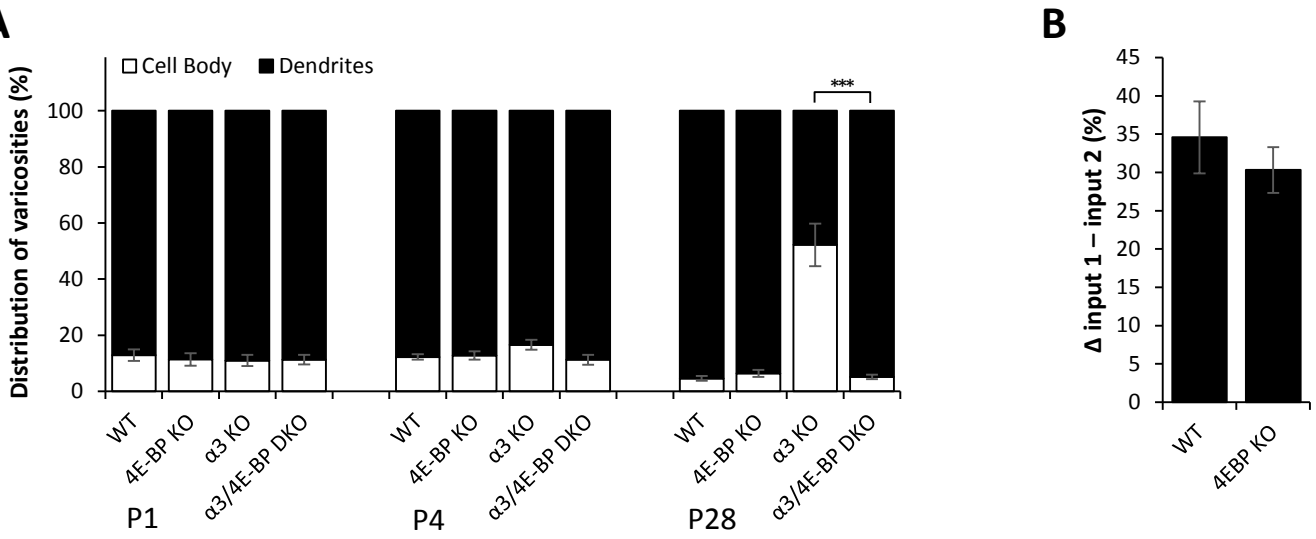

Fig. S4 Chong *et al.*

Figure S4. The distribution of varicosities is restored to the dendrites in α3/4E-BP DKO mice at P28. Related to Figure 5.

(**A**) Average distribution of varicosities on the cell body (open) and dendrites (filled) in WT, 4E-BP KO, α3 KO, and α3/4E-BP DKO SCG at P1, P4 and P28.

(**B**) The average difference in strength between the strongest and second strongest inputs in WT and 4E-BP KO SCG at P28, expressed as a percentage of the maximum compound EPSP.

Error bars represent ± SEM; ***p<0.001. In A, WT: for P1, n=6 neurons (3 mice); for P4, n=9 neurons (5 mice); and for P28, n=10 neurons (4 mice). 4E-BP: for P1 n=6 neurons (3 mice); for P4, n=7 neurons (5 mice); and for P28, n=10 neurons (4 mice). α3 KO: for P1 n=6 (5 mice); for P4, n=10 neurons (4 mice); and for P28, n=11 neurons (4 mice). α3/4E-BP DKO: for P1 n=6 (3 mice); for P4, n=7 neurons (4 mice); and for P28, n=10 neurons (4 mice). In B, WT n=36 neurons, 4E-BP n=33 neurons.

A Molecular Function

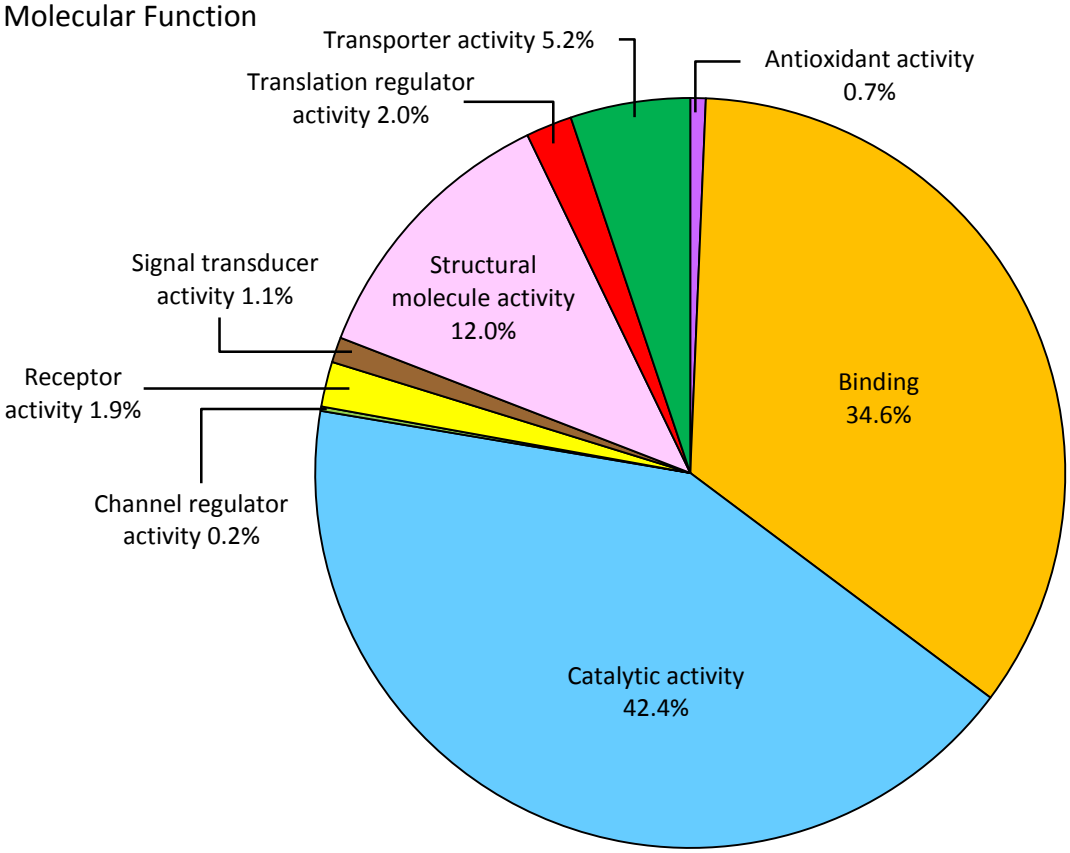

B Protein Class

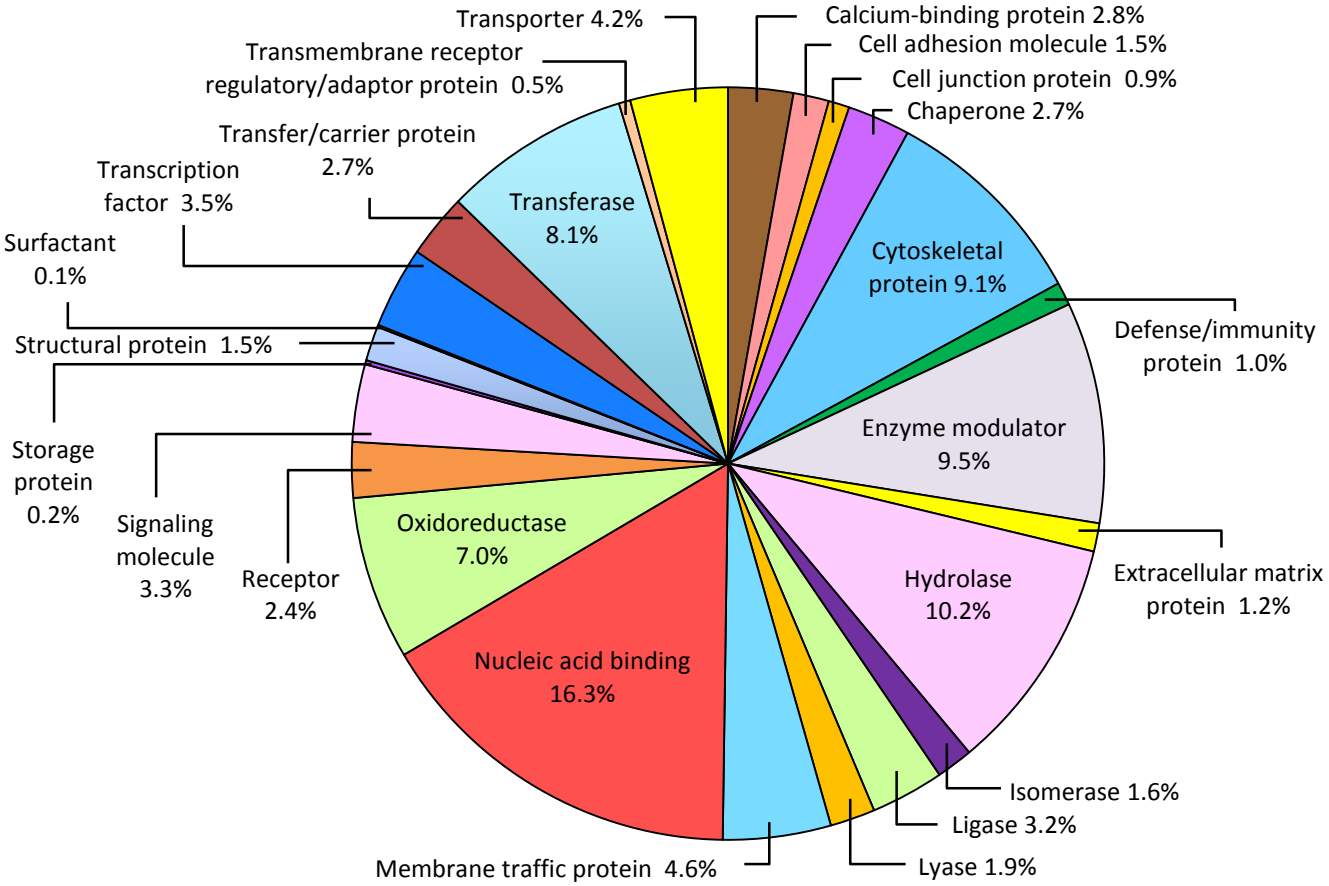

Fig. S5 Chong *et al.*

Figure S5. The classification of 2100 proteins identified in P28 WT SCG. Related to Figure 5.

(**A**&**B**) Pie charts showing the classification of 2100 proteins identified in P28 WT SCG into (**A**) molecular functions, and (**B**) protein classes. Proteins were identified using a data-independent acquisition SWATH MS/MS workflow and classified according to Gene Ontology (GO) terms and PANTHER protein classes.

Gene		Primer sequence (5’ – 3’)
α3	WT	FWD: GTT ATG CAC GGG AAG CCA GGC TGG REV: GAC TGT GAT GAC GAT GGA CAA GGT GAC
	KO	FWD: GTT ATG CAC GGG AAG CCA GGC TGG REV: TGG CGC GAA GGG ACC ACC AAA GAA CGG
4E-BP1	WT	FWD: GAT GGA GTG TCG GAA CTC ACC REV: GAC CTG GAC AGG ACT CAC CGC
	KO	FWD: GCA TCG AGC GAG CAC GTA CTC REV: GAC CTG GAC AGG ACT CAC CGC
4E-BP2	WT	FWD: GGG TGG ACT GTC GGT CTT CTG REV: CAG CAC CTG GTC ATA GCC GTG
	KO	FWD: GCA TCG AGC GAG CAC GTA CTC REV: CAG CAC CTG GTC ATA GCC GTG

Table S1. Forward and reverse primer sequences used for PCR genotyping of α3, 4E-BP1 and 4E-BP2 KO mice. Related to Figure 4 and Supplemental Figure S3.

Gene	Primer sequence (5’ – 3’)
4E-BP1	FWD: AGC CAT TCC TGG GGT CAC TA REV: ATC ATT GCG TCC TAC GGC TG
4E-BP2	FWD: CTG CCC TCT GCC CAG TTA AG REV: TGC TTG GAG ACT GCC CTA GA
GAPDH	FWD: CTG GCA TGG CCT TCC GTG TT REV: TAC TTG GCA GGT TTC TCC AGG CG
18S	FWD: GCA ATT ATT CCC CAT GAA CG REV: GGG ACT TAA TCA ACG CAA GC

Table S2. Forward and reverse primer sequences used for qPCR. Related to Figure 4 and Supplemental Figure S3.

Table S3. Z-scores, z-score ratios, and q-values used to generate the heatmap in Figure 5.

Gene	z-score			α3 KO : WT		α3/4E-BP DKO : WT	
	WT	α3 KO	α3/4E-BP DKO	Ratio	q-value	Ratio	q-value
Acly	1250.5	1942.25	1874.97	1.55	1.08E-07	1.5	1.81E-06
Anp32b	399.8	610.7	617.01	1.53	0.048	1.54	0.018
Anxa5	2915.33	5223.19	5387.85	1.79	1.16E-15	1.85	2.49E-14
Ap2a2	247.34	358.36	340.03	1.45	0.021	1.37	0.278
Apoa1	2924.02	5262.45	8421.88	1.8	1.77E-04	2.88	4.41E-09
Apod	127.19	210.8	257.8	1.66	0.037	2.03	0.157
Arhgdia	1602.77	2313.65	2066.32	1.44	3.34E-04	1.29	0.008
Atic	872.33	1324.71	1120.78	1.52	0.007	1.28	0.002
Atp5a1	3152.5	1567.74	1882.91	0.5	0.007	0.6	2.78E-08
Atp5b	182.91	62.09	121.81	0.34	0.028	0.67	0.238
Atp5c1	413.57	288	293.54	0.7	0.008	0.71	0.305
Atp5j	362.61	208.97	240.97	0.58	0.026	0.66	0.229
Cadm2	149.53	332.15	264.36	2.22	0.006	1.77	0.319
Cda	246.78	369.41	184.57	1.5	0.016	0.75	0.028
Cend1	212.73	101.83	123.41	0.48	0.002	0.58	0.001
Ckb	2518.17	1231.73	1622.96	0.49	0.002	0.64	0.024
Col28a1	1191.56	824.37	1487.35	0.69	0.002	1.25	0.087
Cox5b	967.24	593.47	559.63	0.61	0.033	0.58	0.013
Cpne2	49.04	89.34	112.22	1.82	0.024	2.29	0.277
Ctsb	1064.6	673.32	805.34	0.63	3.00E-05	0.76	0.002
Ddc	943.57	1525.27	1254.44	1.62	1.48E-04	1.33	0.422
Elavl2	640.62	350.58	379.97	0.55	0.005	0.59	0.002
Epdr1	487.08	774.35	549.25	1.59	0.01	1.13	0.571
Fasn	1719.25	2196.54	2206.74	1.28	2.30E-09	1.28	2.3E-06
Fbl	283.6	359.22	301.55	1.27	0.021	1.06	0.532
Fbxo2	451.87	639.45	484.52	1.42	0.01	1.07	0.311
Fkbp1a	1219.7	2053.61	1936.77	1.68	0.001	1.59	2.02E-04
Gda	403.7	980.37	1204.14	2.43	0.002	2.98	6.62E-11
Gmppb	411.7	771.64	458.94	1.87	0.006	1.11	0.346
Gpi	523.14	694.22	619.6	1.33	0.004	1.18	0.515
Gpx1	838.91	1226.97	1345.89	1.46	0.029	1.6	0.097
Hist1h1a	300.51	550.38	807.74	1.83	0.008	2.69	0.007
Hist1h1b	324.5	563.9	723.3	1.74	0.044	2.23	3.50E-05
Hist1h1c	2075.08	3307.83	3830.5	1.59	0.044	1.85	0.001
Hist1h1e	2120.81	2958.81	3303.83	1.4	0.006	1.56	0.007
Hist2h2aa1	225.09	295.46	455.17	1.31	0.029	2.02	0.204
Hmgn2	50.61	98.82	106.94	1.95	2.00E-05	2.11	0.054
Ina	1663.29	1026.06	1130.21	0.62	4.31E-04	0.68	0.079
Krt1	1236.6	548.35	811.24	0.44	1.74E-08	0.66	1.23E-04
Krt10	1498.45	724.91	1171.19	0.48	0.02	0.78	0.116
Krt2	632.05	394.83	448.31	0.62	0.014	0.71	0.187
Krt6a/6b	1032.29	415.01	666.1	0.4	0.005	0.65	0.355
Krt77	1285.23	588.03	838.06	0.46	4.48E-04	0.65	0.003
Krt79	378.5	197.18	252.02	0.52	0.001	0.67	8.00E-06
Lnp	137.96	76.22	85.59	0.55	0.012	0.62	0.186
Mif	1907.87	2727.7	2745.68	1.43	0.008	1.44	0.034
Mtco2	439.93	227.52	296.75	0.52	0.03	0.67	0.343
Myl1	615.39	275.81	371.95	0.45	0.001	0.6	0.003

Table S3 (continued).

Naca	751.28	557.81	556.84	0.74	0.01	0.74	0.062
Ncald	229.29	97.49	96.16	0.43	3.66E-05	0.42	0.005
Nefh	950.5	432.24	414.24	0.45	8.20E-08	0.44	1.43E-08
Nefl	3029.67	1977.93	2040.21	0.65	9.35E-11	0.67	1.33E-09
Npy	129.9	33.06	50.79	0.25	0.039	0.39	0.413
Nudt3	105.6	202.96	179.44	1.92	0.023	1.7	0.427
Omp	594.07	761.61	763.64	1.28	0.028	1.29	0.127
Oxct1	1116.11	814.54	920.08	0.73	0.001	0.82	0.044
Pabpc1	898.41	1240.42	993.25	1.38	0.038	1.11	0.066
Pcnp	237.34	373.99	333.01	1.58	0.041	1.4	0.602
Pdhx	255.47	162.62	208.66	0.64	0.033	0.82	0.349
Pfn2	240.89	327.03	286.13	1.36	0.011	1.19	0.241
Pgp	128.23	190.64	164.13	1.49	0.034	1.28	0.289
Pnp	329.19	495.64	507.25	1.51	0.007	1.54	0.004
Ppia	2699.2	3405.2	3383.34	1.26	5.79E-05	1.25	2.00E-05
Prdx2	6025.87	7602.19	6347.94	1.26	8.33E-05	1.05	0.648
Psma6	581.44	735.78	694.06	1.27	0.014	1.19	0.248
Ptma	232.69	362.75	233.55	1.56	4.45E-04	1	0.386
Pura	1701.36	1194.41	1250.4	0.7	1.92E-04	0.73	0.007
Rbm3	259.32	519.76	567.58	2	0.039	2.19	0.099
Rps14	659.08	897.3	733.44	1.36	0.013	1.11	0.626
Rps5	762.55	561.21	515.19	0.74	0.015	0.68	1.08E-05
Selenbp1	260.2	353.64	394.6	1.36	0.013	1.52	1.70E-05
Serpina1b	377.23	511.03	604.04	1.35	1.20E-05	1.6	0.001
Serpina3k	621.93	927.09	629.82	1.49	0.034	1.01	0.011
Snd1	677.49	856.72	780.93	1.26	0.004	1.15	0.068
Stoml3	268.68	403.21	251.51	1.5	0.039	0.94	0.442
Th	1267.48	896.7	778.87	0.71	0.031	0.61	0.007
Thy1	816	573	489.42	0.7	0.005	0.6	2.02E-04
Tmsb10	3240.45	4483.99	3968.66	1.38	0.008	1.22	0.652
Tpt1	403.12	507.3	394.21	1.26	0.036	0.98	0.403
Tuba1b	1513.21	2513.96	2299.94	1.66	8.81E-08	1.52	5.98E-07
Uqcrc1	666.74	483.92	488.96	0.73	0.007	0.73	0.049
Ybx1	81.76	112.96	107.04	1.38	0.049	1.31	0.062
Ywhae	732.18	1075.49	1099.8	1.47	4.79E-09	1.5	6.02E-06

Contact for Reagent and Resource Sharing

Further information and requests for resources and reagents should be directed to and will be fulfilled by the Lead Contacts, Ellis Cooper (Ellis.Cooper@McGill.ca) or Pejmun Haghighi (phaghighi@buckinstitute.org).

Experimental Model and Subject Details

Mice

Mice with a deletion in the alpha 3 nicotinic subunit gene (Xu *et al*., 1999; referred to as α3 KO) were maintained on an outcrossed background (Krishnaswamy and Cooper, 2009). Briefly, inbred C57BL/6J α3+/- mice were mated to CD-1 WT mice and F1 α3+/- heterozygotes were used as breeders to produce α3 KO mice and WT littermates on a mixed C57BL/6J x CD-1 background. A series of crosses were performed between 4EBP1/2-/- mice (Tsukiyama-Kohara *et al*., 2001; Banko *et al*., 2005; provided by Dr. Nahum Sonenberg, McGill University) and α3 KO mice to generate 4EBP1/2-/-; α3-/- mice (referred to as α3/4E-BP DKO) on a mixed C57BL/6J x CD-1 background. Genotypes for all three genes were determined by PCR (**Supplemental Figure S3A**). Experiments were conducted on both male and female mice and all procedures for animal handling were carried out according to the guidelines of the Canadian Council on Animal Care.

Primary Neuronal Cultures

SCG neurons were cultured as described in Rassadi *et* al., 2005. Briefly, SCG were dissected from P4 α3 KO or WT littermates under sterile conditions. Ganglia were dissociated at 37°C in trypsin (1mg/mL; Worthington, Freehold, NJ) dissolved in 1X HBSS pH 7.4, washed with 1X HBSS, and plated on laminin-coated coverslips in growth media. The growth media consists of L-15 media supplemented with vitamins, cofactors, penicillin–streptomycin, 5% rat serum, and NGF (50 ng/ml). Cultures were treated with cytosine arabinoside (10μm; Sigma Millipore, St. Louis, MO) from days 2 to 4 to eliminate non-neuronal cells, and fed every 3 days.

Method Details

Electrophysiological Recordings

SCG were acutely dissected in oxygenated Tyrode's solution supplemented with glucose (5.6 mM) and choline (0.01 mM) (pH = 7.3–7.4), pinned down with minutia pins on a Sylgard-coated petri dish, mounted on a fixed stage, and viewed through a dissecting microscope (SMZ-10; Nikon, Tokyo, Japan). To record the nerve-evoked postganglionic compound action potential (CAP), we connected the preganglionic nerve to a stimulator (Stimulus Isolator, model A365; World Precision Instruments, Sarasota, FL) with a suction electrode and recorded from the postganglionic trunk with a suction electrode connected to differential amplifier (DP-301; Warner Instruments); the signals were amplified (1000 X), filtered at 300 Hz and 10kHz, and digitized at 10kHz.

To record intracellularly from ganglion cells, we used 80–120 mΩ glass microelectrodes (G150F-4; Warner Instruments, Hamden, CT) made with a DMZ universal puller (Zeitz Instruments, Munich, Germany). Stable intracellular recordings were achieved with a high inertial precision microdrive (Inchworm 8200; EXFO, Quebec, Canada) attached to a micromanipulator (SM11; Narshige, Tokyo, Japan) that drove the electrode through the ganglion. The recording electrode was filled with 1M KAc and connected by a thin silver chlorided wire to the head stage of an Axoclamp 2A amplifier (Axon Instruments, Union City, CA) used in current-clamp mode, and depolarizing or hyperpolarizing constant current pulses were applied through the recording electrode. Membrane voltages were filtered at 3kHz (low-pass cutoff) and 1Hz (high-pass cutoff) and digitized at 50 kHz. On-line stimulation and data acquisition were done with N-Clamp (Neuromatic, UK) and off-line data analysis was performed using Igor Pro software (WaveMetrics, Lake Oswego, OR). To measure dendrites on Ad-α3 infected neurons, intracellular electrodes (60–70 mΩ) were filled with 10mM Alexa Fluor 488 hydrazide (Thermo Fisher Scientific, Waltham, MA) in 200mM KCl.

To measure the convergence of preganglionic axons innervating a sympathetic neuron, the preganglionic nerve was stimulated with voltages of increasing strength while holding the neuron at ~ -90 mV to prevent EPSPs from triggering action potentials. In some experiments, we also included QX314 in the recording electrode to prevent action potentials. At maximal stimulus strength, the $EPSP_{max}$ is the sum of the EPSPs evoked by each of the axons innervating that neuron (Eq. 1). Increasing the strength of the stimulus to the preganglionic nerve activates axons of different threshold which results in discrete jumps in the amplitude of the EPSPs. We used these discrete jumps as a measure of the number of axons innervating the neuron. To isolate the EPSP evoked by individual axons, we averaged at least 10 traces for each discrete jump and subtracted the average EPSP evoked by that axon and all axons of lower threshold from the average EPSP evoked only by axons of lower threshold (Eq. 2).

For N axons innervating a neuron,

$$\mathrm{EPSP}_{max} = \sum_{n=1}^{N} \mathrm{EPSP}_n \qquad \text{Eq. 1}$$

To isolate the $EPSP_n$ evoked by axon n,

$$\mathrm{EPSP}_n = \sum_{n=1}^{n} \mathrm{EPSP}_n - \sum_{n=1}^{n-1} \mathrm{EPSP}_{n-1} \qquad \text{Eq. 2}$$

To calculate the disparity index, DI, for each neuron, we divided the standard deviation, SD, of the EPSPs by the mean EPSP (Hashimoto and Kano, 2003). (Eq. 3.)

$$DI = SD/M \qquad \text{Eq. 3}$$

$$SD = \sqrt{\frac{\sum_{n=1}^{N} (EPSP_n - M)^2}{N-1}}$$

$$M = \mathrm{EPSP}_{max}/N$$

Adenoviruses

Full-length α3 neuronal nAChR subunit cDNA was ligated into pAdTrack-synapsin 1 (Ad-α3/Syn), and replication-deficient viral vectors were made according to He *et al*. (1998), as described previously (Krishnaswamy and Cooper, 2009). The synapsin promoter was only active in SCG neurons for ~2 weeks; to overexpress α3 for longer times, we used the human ubiquitin C promoter (Schorpp *et al*., 1996). Viruses were titered in duplicate with Adeno-X Rapid Titer Kit, (Clontech Lab, Mountain View, CA).

We infected mice with either Ad-α3/Syn or Ad-α3/Ubi adenovirus at a concentration of ~10^7 pfu/mL diluted in 1X PBS. For P28 α3 KO or α3/4E-BP DKO and P60 α3 KO mice, 200-300 µL was injected into the tail vein (IV). For P0-1 pups, we injected ~50 µL into the temporal vein, and for P8-9 pups, we injected 100-150 µL into the intraperitoneal cavity (IP).

Lipophilic Tracer Labeling

We used lipophilic tracers DiI and DiO (Thermo Fisher Scientific) to sparsely label a random subset of preganglionic axons and postsynaptic neurons in the SCG. When used to quantify dendritic morphologies, this method is preferable to labelling with intracellular dye injection because it avoids selection bias for neurons with large cell bodies. Briefly, freshly dissected ganglia with intact pre- and post-ganglionic nerves were fixed in 1% PFA (pH 7.4) in 0.1M PB for 2 hours at room temperature (RT) and embedded in 3% agarose Type I-B (Sigma Millipore) dissolved in 1X PBS, and a razor blade was used to slice through the pre- and post- ganglionic nerves to expose a cross-sectional area of the nerve. Platinum wires were used to gently apply fine crystals of DiI to the preganglionic nerve, and DiO to the postganglionic

nerve. After labelling, ganglia were kept in the dark in 1X PBS for 5 - 6 days to allow for tracers to diffuse along the axons. Ganglia were sliced into 100 μm sections with the Compresstome VF-200 (Precisionary Instruments Inc., Greenville, NC) using a solid zirconia ceramic injector blade (Cadence Inc., Staunton, VA). Sections were either mounted with Vectashield (Vector Laboratories, Burlingame, CA) and immediately imaged, or first processed with immunohistochemistry before mounting and imaging.

Immunohistochemistry

SCG were fixed, embedded, and sliced into 100 μm sections with the Compresstome VF-200, as above. Fixation and blocking were performed at room temperature.

VAChT staining on DiO-labelled or Alexa Fluor 488-filled neurons: We immunostained for VAChT on DiO-labelled neurons in fixed sections, or on Alexa Fluor 488-filled neurons in ganglia that were then fixed in 1% PFA in 0.1M PB for 1 hr and sectioned. Sections were blocked in 10% normal donkey serum (DS) (Millipore), and 0.3% Tween 20 (Fisher Scientific) in 1X PBS (blocking solution) for 2 hr, and then, incubated in primary antibodies in blocking solution at 4°C for 48 hr, and then in secondary antibodies in 10% DS at RT for 2 hr, and imaged. Primary antibody: Rabbit anti-VAChT (1:3000; Synaptic Systems); Secondary antibody: Alexa Fluor 647 donkey anti-rabbit (1:500; Thermo Fisher Scientific).

P-4E-BP1, 4E-BP1 and MAP-1A staining: SCG were immediately fixed in 2% PFA in 0.1M PB with 5mM EGTA for 1 hr and then sectioned. Sections were blocked in 10% DS, 0.3% Tween 20 and 0.05% Triton X-100 in 1X PBS (blocking solution) for 1 hr and incubated in primary antibodies (P-4E-BP1 or 4E-BP1 with MAP-1A) in blocking solution at 4°C for 48 hours, then in secondary antibodies in 10% DS at RT for 1 hr, and mounted for imaging. WT and α3 KO samples were processed in parallel. Primary antibodies: Rabbit anti-P-4E-BP1 (1:600; Cell Signaling, Danvers, MA), rabbit anti-4E-BP1 (1:600; Cell Signaling), goat anti-MAP-1A (1:360; Santa Cruz Biotechnology, Dallas, TX); Secondary antibodies:

TRITC donkey anti-rabbit (1:500; Jackson ImmunoResearch Laboratories) and Alexa Fluor 647 donkey anti-goat (1:500; Thermo Fisher Scientific).

VAChT and PSD-93: SCG were immediately fixed in 2% PFA in 0.1M PB (pH 6) for 10 minutes and then sectioned. Sections were blocked in 10% DS, and 0.3% Tween 20 in 1X PBS (blocking solution) for 2 hr, then incubated in primary antibodies in blocking solution at 4°C for 48 hr, and then in secondary antibodies in 10% DS at RT for 1 hr, and imaged. Primary antibodies: Rabbit anti-VAChT (1:3000; Cell Signaling, Danvers, MA), mouse anti-PSD-93 (1:300; NeuroMab, Davis, CA); Secondary antibodies: Alexa Fluor 647 donkey anti-rabbit (1:500; Thermo Fisher Scientific) and Alexa Fluor 568 goat anti-mouse IgG1 (1:500; Thermo Fisher Scientific).

Immunocytochemistry

Cultured SCG neurons (14 days *in vitro*) were fixed and permeabilized with cold 100% methanol for 10 mins at -20°C, rinsed with 1X PBS, blocked in 10% DS in 1X PBS for 1 hr, incubated in primary antibody mouse anti-MAP-2 (1:500; Sigma Millipore) in blocking solution overnight at 4°C, then in secondary antibody Alexa Fluor 568 goat anti-mouse IgG1 (1:500; Thermo Fisher Scientific) for 1 hr at room temperature, and imaged.

Image Acquisition and Analysis

Images were acquired on an upright confocal microscope (BX-61W, Olympus) with a 60X, NA 1.42 PlanApo N oil-immersion objective at a scan speed of 8 μs/pixel and an image depth of 12 bits. Laser lines were activated sequentially to avoid bleed-through of signals. All analysis was performed with ImageJ (NIH, Bethesda, MD).

Dendrite analysis: Images of DiO-labelled neurons were acquired at a pixel size of 0.172 μm/pixel (1024 x 1024 pixels) and an optical thickness of 0.37 μm/slice. Only neurons with complete dendritic arbors and an identifiable axon were analyzed. For images of isolated neurons, we removed all DiO-labelled neurites

that were not connected to the neuron of interest, as determined from 3D reconstructions. To quantify the length and number of dendritic branches, we reconstructed neurons in 3D and used the Simple Neurite Tracer plugin (Longair *et al*., 2011) to trace dendrites. Primary dendrites were categorized as those directly leaving the cell body, while secondary branches extended off primary dendrites. Thin protrusions shorter than 5 µm were considered dendritic filopodia and not counted as branches. For neurons with a dendritic arbor that extended beyond one field of view, neighbouring z-stacks were acquired and stitched together with XuvTools (Emmenlauer *et al*., 2009).

Synaptic targeting: Images were acquired at a pixel size of 0.172 µm/pixel (1024 x 1024 pixels), and an optical thickness of 0.36 µm/slice. To examine synaptic targeting, we identified VAChT puncta located on a neuron of interest on each plane of a z-stack. VAChT puncta that co-localized with the DiO membrane label, were at least 0.5 µm in diameter, and spanned at least two optical slices were counted as putative synapses.

Preganglionic axonal targeting: Images were acquired at a pixel size of 0.188 µm/pixel (1024 x 1024 pixels), optical thickness was 0.4 µm/slice. To estimate the percentage of the cell body surface covered by an axon, on each plane of the cell body, we measured the circumference of the cell body (DiO labelled from postganglionic nerve), and the proportion of the cell body circumference occupied by an axon (DiI labelled from preganglionic nerve) on that plane. The total surface area was calculated from the circumference of the cell body on each plane multiplied by the optical thickness.

P-4E-BP1, 4E-BP1 and MAP-1A fluorescence intensity: A z-stack of 20 images were acquired at a pixel size of 0.22 µm/pixel (800 x 800 pixels), and optical thickness was 0.47 µm/slice. All image acquisition parameters (HV, gain, offset, laser power) were kept constant between samples. For intensity analysis, each stack was used to generate a summed z-projection. Regions of interest (ROI), each consisting of one neuronal cell body, excluding the nucleus, were selected from the MAP-1A channel. Average

fluorescence intensity for each ROI was measured from the MAP-1A channel, and ROI were transferred to the P-4E-BP1 or 4E-BP1 channel to measure the corresponding fluorescence intensity.

Proteomics

Chemicals: Acetonitrile and water were obtained from Burdick & Jackson (Muskegon, MI). Reagents for protein chemistry including iodoacetamide, dithiothreitol (DTT), ammonium bicarbonate, formic acid (FA), and urea were purchased from Sigma Aldrich (St. Louis, MO). Sequencing grade trypsin was purchased from Promega (Madison, WI). HLB Oasis SPE cartridges were purchased from Waters (Milford, MA).

Superior Cervical Ganglia Sample Preparation for Mass Spectrometry – Digestion: For mass spectrometric analysis isolated frozen ganglia tissue pellets in PBS from WT and 3 different knock-out mice, 4EBP-KO, alpha-3-KO, and 4EBP/ alpha-3–double KO (also referred to as DKO) were processed. Mice were four weeks old and 6 ganglia were pooled into one sample, with a total of 3 biological replicates per each of the mouse strain. Ganglia were re-suspended in PBS containing 1X Roche Protease and Phosphatase inhibitor cocktail and lysed using a bead-beater and sonication. Samples were concentrated using 3 kDa centrifugal filters and transferred into a solution of 8M urea/100 mM Tris pH 8, and protein quantitation was performed using a BCA Protein Assay Kit (Pierce #23225, Waltham, MA). An aliquot of 10-20 µg from each sample was then brought to equal volume with 100 mM Tris buffer at pH 8. The protein mixtures were reduced with 20 mM DTT (37°C for 1 hour), and subsequently alkylated with 40 mM iodoacetamide (30 minutes at RT in the dark). Samples were diluted 10-fold with 100 mM Tris pH 8.0 and incubated overnight at 37°C with sequencing grade trypsin (Promega) added at a 1:50 enzyme:substrate ratio (wt/wt). The peptide supernatants were then collected and desalted with Oasis HLB 30 mg Sorbent Cartridges (Waters #186003908, Milford, MA) (Keshishian et al. 2007), concentrated and re-suspended in a solution containing mass spectrometric 'Hyper Reaction Monitoring' peptide standards (HRM, Biognosys #Kit-3003, Switzerland) and 0.2% formic acid in water.

Mass Spectrometry: Samples were analyzed by reverse-phase HPLC-ESI-MS/MS using the Eksigent Ultra Plus nano-LC 2D HPLC system (Dublin, CA) combined with a cHiPLC System, which was directly connected to a quadrupole time-of-flight SCIEX TripleTOF 6600 mass spectrometer (SCIEX, Redwood City, CA). Typically, mass resolution in precursor scans was ~ 45,000 (TripleTOF 6600), while fragment ion resolution was ~15,000 in 'high sensitivity' product ion scan mode. After injection, peptide mixtures were transferred onto a C18 pre-column chip (200 µm x 6 mm ChromXP C18-CL chip, 3 µm, 300 Å, SCIEX) and washed at 2 µl/min for 10 min with the loading solvent (H_2O/0.1% formic acid) for desalting. Subsequently, peptides were transferred to the 75 µm x 15 cm ChromXP C18-CL chip, 3 µm, 300 Å, (SCIEX), and eluted at a flow rate of 300 nL/min with a 3 h gradient using aqueous and acetonitrile solvent buffers.

For spectral library building, initial data-dependent acquisitions (DDA) were carried out to obtain MS/MS spectra for the 30 most abundant precursor ions (100 msec per MS/MS) following each survey MS1 scan (250 msec), yielding a total cycle time of 3.3 sec as previously described (Kuhn et al. 2014; Schilling et al. 2012; Schilling et al. 2015). For collision induced dissociation tandem mass spectrometry (CID-MS/MS), the mass window for precursor ion selection of the quadrupole mass analyzer was set to ± 1 *m/z* using the Analyst 1.7 (build 96) software. Subsequently, for label-free relative quantification all study samples were analyzed by data-independent acquisitions (DIA), or specifically variable window SWATH acquisitions. In these SWATH acquisitions (Kuhn et al. 2014; Rardin et al. 2015), instead of the Q1 quadrupole transmitting a narrow mass range through to the collision cell, windows of variable width (5 to 90 *m/z*) are passed in incremental steps over the full mass range (*m/z* 400-1250). The cycle time of 3.2 sec includes a 250 msec precursor ion scan followed by 45 msec accumulation time for each of the 64 SWATH segments. The variable windows were determined according to the complexity of the typical MS1 ion current observed within a certain *m/z* range using a SCIEX 'variable window calculator' algorithm (i.e. more narrow windows were chosen in 'busy' *m/z* ranges, wide windows in *m/z* ranges with few eluting precursor ions)(Schilling, Gibson, and Hunter 2017). SWATH MS2 produces complex MS/MS spectra which are a composite of all the analytes within each selected Q1 m/z window.

Mass Spectrometric Data Processing and Bioinformatics: Mass spectrometric data from data dependent acquisitions was analyzed using the database search engine ProteinPilot (SCIEX 5.0)(Shilov et al. 2007) using the Paragon algorithm. The following sample parameters were used: trypsin digestion, cysteine alkylation set to iodoacetamide, urea denaturation, and species *Mus musculus*. Trypsin specificity was assumed as C-terminal cleavage at lysine and arginine. Processing parameters were set to "Biological modification" and a thorough ID search effort was used. All DDA data files were searched using the SwissProt 2016_07 database (species: *M. musculus*). For Protein Pilot searches, to assess and restrict rates of false positive peptide/protein identifications, we used the (PSPEP) tool available in ProteinPilot 5.0 (Shilov et al. 2007), which automatically creates a concatenated forward and reverse decoy database. For database searches, a cut-off peptide confidence value of 99 was chosen. The Protein Pilot false discovery rate (FDR) analysis tool PSPEP provided a global FDR of 1% and a local FDR at 1% in all cases.

SWATH acquisitions were quantitatively processed using the proprietary Spectronaut v11 (11.0.15038.2.22948) software (Bruderer et al. 2016) from Biognosys. Quantitative SWATH MS2 data analysis was based on extracted ion chromatograms (XICs) of 6-10 of the most abundant fragment ions in the identified spectra. Relative quantification was performed comparing different conditions (WT and KO mice) assessing fold changes for proteins from the investigated mouse lines. Typically ganglia were pooled from 3 mice (2 ganglia per mouse providing a total of 6 ganglia) into one pooled biological replicate sample, and three of such pooled biological replicates per each of the four mouse strains were investigated and compared. Significance was assessed using FDR corrected q-values<0.05. See Data Accession (below) for quantitative results from mass spectrometric SWATH analysis.

Data Accession: The supplementary files provide further insights into the quantitative SWATH results. All raw files are uploaded to the Center for Computational Mass Spectrometry, MassIVE, and can be downloaded using the following link: ftp://MSV000081386@massive.ucsd.edu (MassIVE ID number: MSV000081386 and password: winter; ProteomeXchange Accession PXD007141). Data uploads include

mass spectrometric details for proteins and peptides that were identified and quantified by mass spectrometric analysis.

Heatmap: To generate the heatmap in Figure 5, we first identified proteins that were expressed at significantly different levels between α3 KO and WT SCG (±1.25x at q-value <0.05). For each of the 83 proteins identified to be differentially expressed, we calculated the $\log_2$ z-score ratio between the expression level in α3 KO SCG and the corresponding level in WT SCG, and between α3/4E-BP DKO SCG and WT SCG. We plotted the ratios using the gplots package (https://cran.r-project.org/package=gplots) in R (http://www.R-project.org).

Ultrastructural studies

Ganglia were dissected and fixed in 2% PFA/2% glutaraldehyde in 0.1M PB for 30 minutes at room temperature, cut in half to improve penetration and fixed for an additional 90 minutes. After fixation, ganglia were rinsed with 0.1M PB for 30 minutes, and incubated in 1% osmium tetroxide/1.5% potassium ferricyanide in H_2O for 1 hour at room temperature. Ganglia were rinsed briefly with H_2O to remove osmium tetroxide, and dehydrated in a graded series of ethanol concentrations from 30% to 100%, where each interval lasted 10 minutes, with the 100% ethanol step repeated 3 times. After dehydration, ganglia were incubated in 100% propylene oxide for 15 minutes twice, and incubated in a propylene oxide/Embed812 mixture at a ratio of 1:1, 1:2, and 1:3 for 1 hour, 2 hours and overnight respectively, and polymerized in Embed812 at 60C for 24 hours. Thin sections of ganglia were cut on an ultramicrotome, stained with 2% aqueous uranyl acetate and 3% lead citrate, and viewed with a Philips (Holland) EM410 electron microscope. To capture digital images, we used a Megaview 2 cooled-CCD camera at 10C and a GraBIT digital input board with analySIS analysis software (Olympus).

4E-BP1 and 4E-BP2 mRNA expression

RNA extraction and qPCR validation was performed in accordance with the MIQE guidelines (Bustin *et al*., 2009; Taylor *et al*., 2010).

RNA extraction: SCG from P28 WT mice were dissected and immediately flash frozen in liquid nitrogen. For cerebellum, P28 WT mice were perfused with oxygenated aCSF made with DEPC-treated H_2O, the cerebella were quickly removed, and ~200μm of the dorsal surface (lobes ~VI –IX) was isolated to minimize contribution of granule cell layer, and immediately flash frozen in liquid nitrogen. Total RNA from SCG and cerebella were extracted in parallel using the RNeasy Mini Kit (Qiagen). Frozen tissue was homogenized (Polytron PT 2100, Kinematica, Luzern, Switzerland) in buffer RLT with β-mercaptoethanol. Homogenates were processed according to the RNeasy Mini Kit protocol, and included a DNase I (Qiagen) treatment step to avoid contamination from genomic DNA. RNA quantity and purity was assessed with a NanoDrop2000c (NanoDrop, Wilmington, DE), and RNA integrity was assessed by running 400ng on a gel. 260/230 and 260/280 values were consistently >2.0, and 28S and 18S rRNA bands were consistently clear and sharp, with the 28S band approximately twice as intense as the 18S band. Reverse transcription (iScript Reverse Transcription Supermix for RT-qPCR, Bio-Rad, Hercules, CA) was performed immediately after RNA extraction, and used 200ng of RNA per reaction volume of 20μL. No-reverse transcriptase controls were included for each reaction to test for contamination from genomic DNA. cDNA was stored at -20°C.

qPCR: qPCRs were performed using SsoFast EvaGreen (Bio-Rad) on the Eco Real-Time PCR System (Illumina, San Diego, CA). Cycling parameters were as follows: UDG incubation 2mins at 50°C; Polymerase activation 30s at 95°C; PCR cycling (5s at 95°C, 15s at 60°C) for 40 cycles. Standard curves were generated from an 8-point 4X serial dilution of a mixed sample of SCG and cerebellar cDNA to determine primer efficiencies. All primers were 90-100% efficient at an annealing temperature of 60°C. See Table S2 for primer sequences. To compare SCG and cerebellum, samples were normalized to the geometric mean of the reference genes GAPDH and 18S. The stability value determined by NormFinder (Andersen *et al*., 2004) for the combination of GAPDH and 18S was 0.351. To estimate a ratio between 4E-BP1 and 4E-BP2 mRNA levels, we first generated standard curves from a 6-point serial dilution of

known copy numbers of 4E-BP1 and 4E-BP2 cDNA to ensure that both primer pairs and respective amplicons respond in a near-identical manner. See Table S2 for primer sequences. Each reaction contained 4μL of 256X-diluted cDNA in a total reaction volume of 10μL. Samples were run in duplicates, and no-reverse transcriptase and no template controls consistently showed no amplification.

Quantification and Statistical Analysis

Values of n and p-values are reported in the Figures and corresponding figure legends. In all figures, error bars represent ± SEM, *$p<0.05$, ***$p<0.001$. To test for statistical differences between two samples, we used unpaired two-tailed t tests assuming equal variance. To test for statistical differences between three or more samples, we used a one-way ANOVA to determine if one or more samples were significantly different. If the p-value calculated from the F-statistic was less than 0.05, we used a post-hoc Tukey HSD test to identify which pairs of samples were significantly different from each other.

Andersen, C.L., Jensen, J.L., Ørntoft, T.F. (2004). Normalization of real-time quantitative reverse transcription-PCR data: a model-based variance estimation approach to identify genes suited for normalization, applied to bladder and colon cancer data sets. Cancer Research *64*, 5245-50.

Bruderer, R., Bernhardt, O.M., Gandhi, T., Reiter, L. (2016). High-precision iRT prediction in the targeted analysis of data-independent acquisition and its impact on identification and quantitation. Proteomics *16*: 2246–2256.

Bustin, S.A., Benes, V., Garson, J.A., Hellemans, J., Huggett, J., Kubista, M., Mueller, R., Nolan, T., Pfaffl, M.W., Shipley, G. L., Vandesompele, J., and Wittwer, C.T. (2009). The MIQE Guidelines: Minimum Information for Publication of Quantitative Real-Time PCR Experiments. Clinical Chemistry *55*, 611–622.

Emmenlauer, M., Ronneberger, O., Ponti, A., Schwarb, P., Griffa, A., Filippi, A., Nitschke, R., Driever, W., and Burkhardt, H. (2009). XuvTools: free, fast and reliable stitching of large 3D datasets. Journal of Microscopy *233*, 42–60.

Gillet, L.C., Navarro, P., Tate, S., Rost, H., Selevsek, N., Reiter, L., Bonner, R., Aebersold, R. (2012). Targeted data extraction of the MS/MS spectra generated by data-independent acquisition: a new concept for consistent and accurate proteome analysis. Mol Cell Proteomics *11*: O111 016717.

He, T.-C., Zhou, S., Da Costa, L.T., Yu, J., Kinzler, K.W., and Vogelstein, B. (1998). A simplified system for generating recombinant adenoviruses. Proceedings of the National Academy of Sciences *95*, 2509–2514.

Keshishian, H., Addona, T., Burgess, M., Kuhn, E., Carr, S.A. (2007). Quantitative, multiplexed assays for low abundance proteins in plasma by targeted mass spectrometry and stable isotope dilution. Mol Cell Proteomics *6*: 2212–2229.

Kuhn, M. L., Zemaitaitis, B., Hu, L.I., Sahu, A., Sorensen, D., Minasov, G., Lima, B.P., Scholle, M., Mrksich, M., Anderson, W.F., Gibson, B.W., Schilling, B., Wolfe, A.J. (2014). Structural, kinetic and proteomic characterization of acetyl phosphate-dependent bacterial protein acetylation. PLoS One *9*: e94816.

Longair, M.H., Baker, D.A., and Armstrong, J.D. (2011). Simple Neurite Tracer: open source software for reconstruction, visualization and analysis of neuronal processes. Bioinformatics *27*, 2453–2454.

Meyer, J.G., D'Souza, A.K., Sorensen, D.J., Rardin, M.J., Wolfe, A.J., Gibson, B.W., Schilling, B. (2016). Quantification of Lysine Acetylation and Succinylation Stoichiometry in Proteins Using Mass Spectrometric Data-Independent Acquisitions (SWATH). J Am Soc Mass Spectrom *27*: 1758–1771.

R Core Team (2013). R: A language and environment for statistical computing. R Foundation for Statistical Computing, Vienna, Austria. ISBN 3-900051-07-0, URL http://www.R-project.org/.

Rardin, M.J., Schilling, B., Cheng, L.Y., MacLean, B.X., Sorensen, D.J., Sahu, A.K., MacCoss, M.J., Vitek, O., Gibson, B.W. (2015). MS1 Peptide Ion Intensity Chromatograms in MS2 (SWATH) Data Independent Acquisitions. Improving Post Acquisition Analysis of Proteomic Experiments. Mol Cell Proteomics *14*: 2405–2419.

Schilling, B., Christensen, D., Davis, R., Sahu, A.K., Hu, L.I., Walker-Peddakotla, A., Sorensen, D.J., Zemaitaitis, B., Gibson, B.W., Wolfe, A.J. (2015). Protein acetylation dynamics in response to carbon overflow in Escherichia coli. Mol Microbiol *98*: 847–863.

Schilling, B., Gibson, B.W., Hunter, C.L. (2017). Generation of High-Quality SWATH(R) Acquisition Data for Label-free Quantitative Proteomics Studies Using TripleTOF(R) Mass Spectrometers. Methods Mol Biol *1550*: 223–233.

Schilling, B., Rardin, M.J., MacLean, B.X., Zawadzka, A.M., Frewen, B.E., Cusack, M.P., Sorensen, D.J., Bereman, M.S., Jing, E., Wu, C.C., Verdin, E., Kahn, C.R., Maccoss, M.J., Gibson, B.W. (2012). Platform-independent and label-free quantitation of proteomic data using MS1 extracted ion chromatograms in skyline: application to protein acetylation and phosphorylation. Mol Cell Proteomics *11*: 202–214.

Shilov, I.V., Seymour, S.L., Patel, A.A., Loboda, A., Tang, W.H., Keating, S.P., Hunter, C.L., Nuwaysir, L.M., Schaeffer, D.A. (2007). The Paragon Algorithm, a next generation search engine that uses sequence temperature values and feature probabilities to identify peptides from tandem mass spectra. Mol Cell Proteomics *6*: 1638–1655.

Taylor, S., Wakem, M., Dijkman, G., Alsarraj, M., and Nguyen, M. (2010). A practical approach to RT-qPCR—Publishing data that conform to the MIQE guidelines. Methods *50*, S1–S5.

Warnes, G.R., Bolker, B., Bonebakker, L., Gentleman, R., Huber,W., Liaw, A., Lumley, T., Maechler, M., Magnusson, A., Moeller, S., Schwartz, M., Venables, B. (2016) gplots: Various R programming tools for plotting data. R package version 3.0.1, URL https://cran.r-project.org/package=gplots.